ACS APPLIED MATERIALS & INTERFACES

Research Article

www.acsami.org

Selective Growth of n-Type Nanoparticles on p-Type Semiconductors for Z-Scheme Photocatalysis

Masahiro Miyauchi,* Yuuya Nukui, Daiki Atarashi, and Etsuo Sakai

Department of Metallurgy and Ceramic Science, Graduate School of Science and Engineering, Tokyo Institute of Technology, 2-12-1 Ookayama, Meguro-ku, Tokyo 152-8552, Japan

Supporting Information

ABSTRACT: Nanoparticles of an n-type WO_3 semiconductor were segregated on the surface of p-type $CaFe_2O_4$ particles by a heterogeneous nucleation process under controlled hydrothermal conditions. By use of this approach, WO_3 nanoparticles were selectively deposited on the surface of $CaFe_2O_4$, resulting in a significant increase in the photocatalytic reaction rate of the $WO_3/CaFe_2O_4$ composite for the decomposition of gaseous acetaldehyde under visible-light irradiation. The high visible-light activity of the $WO_3/CaFe_2O_4$ composite was due to efficient charge recombination through the junctions that formed between the two semiconductors.

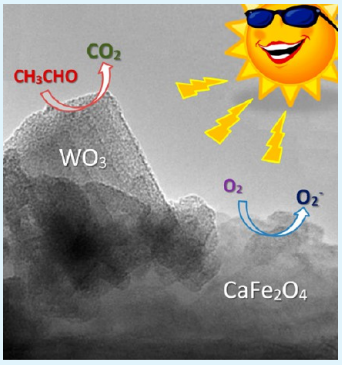

KEYWORDS: *phototocatalysis, WO_3, $CaFe_2O_4$, Z-scheme*

INTRODUCTION

Photocatalysts convert solar energy into useful energy forms and are widely used for energy production and environmental purification applications.[1−8] Efficient photocatalytic reactions require that photogenerated electrons and holes have sufficiently high reduction and oxidation powers, respectively. In the case of the photocatalyst-mediated decomposition of air pollutants, photogenerated holes react with organic substances or hydroxyl species to generate $OH^{\bullet}$ radicals, while photogenerated electrons are trapped by oxygen molecules in air. For these reactions to proceed, the potential of conduction band electrons must be more negative than −0.046 V (vs NHE at pH 0),[9] which equals the redox potential for the production of O_2^- radicals by the one-electron reduction reaction of oxygen. In addition, the potential of holes in the valence band must be more positive than +2.8 V (vs NHE at pH 0) to generate $OH^{\bullet}$ radicals.[10] Acetaldehyde is a typical volatile organic contaminant and is converted to acetic acid at a redox potential of +2.56 V by a thermodynamic consideration. Therefore, to decompose organic contaminants in air using a semiconductor photocatalyst, a theoretical minimum band gap value of +2.8 eV is required. However, the required band gap value is typically larger than the theoretical minimum, as an overpotential is required for the decomposition reactions to proceed. Thus, single-component visible-light-sensitive photocatalysts for environmental purification applications can only utilize photons below a wavelength of 450 nm, which represents only part of the solar light spectrum and therefore drastically reduces reaction efficiency.

To overcome the limitation of single-component photocatalysts, it is possible to construct Z-scheme photocatalysis systems with increased visible-light absorption by introducing heterogeneous semiconductors. Although Z-scheme systems require two photons for each reactant, it is possible to match their band diagram with the solar light spectrum and utilize more photons than single-component photocatalysts, which are only activated below a wavelength of 450 nm. Previous studies adopted Z-scheme systems with visible-light-region sensitivity for various photocatalytic reactions, including water splitting[11−15] CO_2 reduction,[16,17] and oxidation of organic contaminants.[18−23]

Among heterogeneous Z-scheme semiconductor systems, p-type cathode, such as $CaFe_2O_4$, and n-type anode, such as TiO_2 or WO_3, mediate various photocatalytic reactions, including water-splitting,[24] organic contaminant decomposition,[25] and superhydrophilic reactions.[26] The conduction band of $CaFe_2O_4$ is much more negative than that of Fe_2O_3, although both iron oxide compounds have narrow band gap values (1.9 eV).[27] Further, $CaFe_2O_4$ has been reported as a photocatalyst for water-splitting reactions.[24,28−31] In contrast, WO_3 has a band gap value of 2.5−2.8 eV[32−34] and a valence band that is sufficiently positive to oxidize OH^- groups for oxygen evolution in the water splitting reaction and also organic contaminants, such as acetaldehyde and 2-propanol.[35−38] Efficient photocatalytic reactions in Z-scheme systems require the formation of heterojunctions between the two semiconductors. Notably, free particles away from the other

Received: July 20, 2013
Accepted: September 3, 2013
Published: September 3, 2013

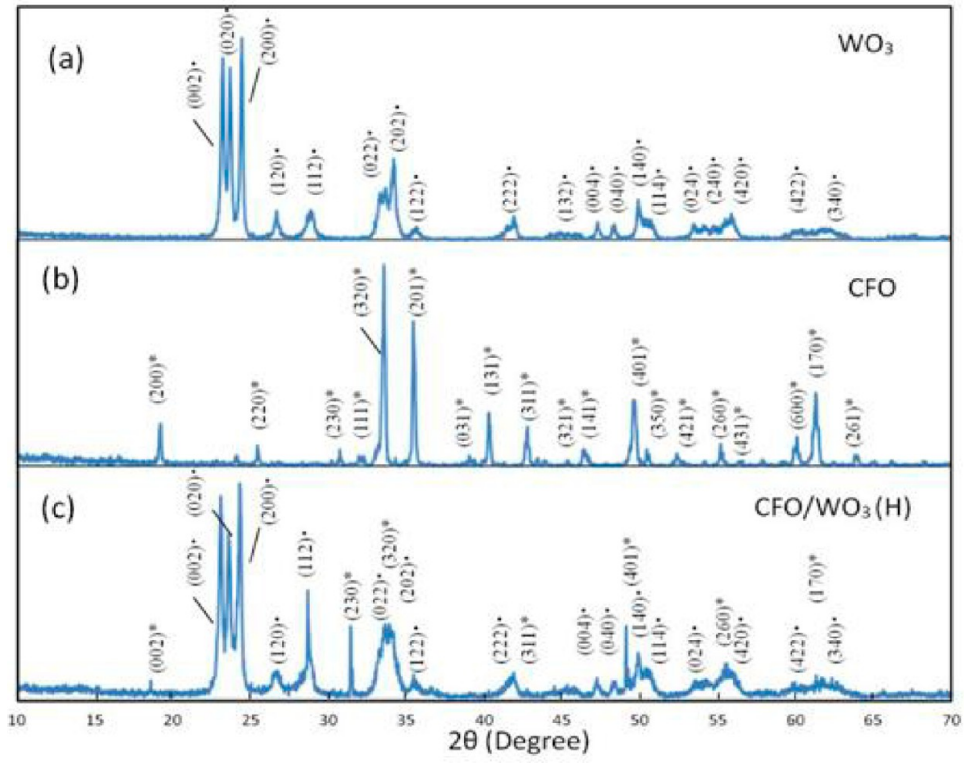

Figure 1. XRD patterns of WO_3 (a), CFO (b), and CFO/WO_3(H) (c). The weight percentage of CFO in CFO/WO_3(H) was 10%: (●) WO_3, (∗) CFO.

semiconductor particles do not contribute to the photocatalytic reactions mediated by Z-scheme systems.

Herein, a model system composed of WO_3 and $CaFe_2O_4$ as n- and p-type semiconductors, respectively, was constructed to determine if the selective deposition of heterogeneous semiconductor particles is effective for developing Z-scheme-type photocatalysts with high visible-light activity. WO_3 nanoparticles were selectively segregated onto the surface of $CaFe_2O_4$ particles using a heterogeneous nucleation process under controlled hydrothermal conditions. We also attempted to determine the optimum hydrothermal conditions to selectively deposit WO_3 nanoparticles on the surface of $CaFe_2O_4$ for the efficient photocatalytic decomposition of gaseous acetaldehyde under visible-light irradiation.

EXPERIMENTAL SECTION

Single-component $CaFe_2O_4$ (CFO) powder was synthesized by a solid-state reaction using calcium acetate monohydrate and iron(III) nitrate anhydrate (Wako Pure Chemical Industries, Ltd.) as precursors. In a typical experiment, 0.88 g of calcium acetate monohydrate and 4.04 g of iron nitrate anhydrate were dissolved in 20 mL of pure water, and 0.30 g of polyethylene glycol (PEG, molecular weight of 3600−4000 kg/mol) was then added to the solution. The solvent was evaporated at 453 K, forming a gray gel-like powder, which was then calcined at 723 K for 2 h and 1323 K for 10 h to form fine CFO powder. WO_3 nanoparticles were deposited on CFO by hydrothermal treatment in an aqueous solution of 20 mL of pure water containing 0.089 g of CFO powder and 0.862 g of tungsten acid (H_2WO_4, Kanto Kagaku, Ltd.; CFO/WO_3 mass ratio of 1:9), which was used as the precursor for WO_3 particles. The aqueous solution was heated at 453 K for 12 h in an autoclave, and the formed solid and solution were separated by centrifugation at 6000 rpm for 8 min. The collected solid was washed several times with distilled water and then dried at 333 K for 20 h in an oven. The CFO/WO_3 composite obtained by this hydrothermal reaction was termed "CFO/WO_3(H)". In addition, pure WO_3 particles were synthesized by the same hydrothermal treatment method in an aqueous solution containing H_2WO_4. For comparison with the hydrothermally synthesized composite, the WO_3/CFO composite was also prepared by mechanical mixing of CFO and WO_3 powder in a quartz mortar in the presence of a small amount of pure water. After being ground with a pestle, the material was dried at 333 K for 20 h to obtain the mechanically mixed composite, which was termed "CFO/WO_3(M)".

X-ray powder diffraction (XRD) patterns were measured by a diffractometer (MXP3 II, Bruker AXS Ltd.) with Cu Kα X-rays. The morphology of the materials was observed using field-emission scanning electron microscopy (FE-SEM, S-4500, Hitachi Ltd.) and transmission electron microscopy (TEM, HF-2000, Hitachi Ltd.). The absorption spectra of the photocatalysts were measured on a UV−visible (UV−vis) spectrophotometer (V-660, JASCO Ltd.) equipped with an integration sphere unit using diffuse reflection mode. The ζ potential of synthesized CFO was recorded on an electrophoretic light-scattering spectrophotometer (ELS-Z, Otsuka Electronics Ltd.). The pH of the sample for the ζ-potential measurement was adjusted using aqueous solutions of sodium hydroxide (NaOH) and hydrochloric acid (HCl). The specific surface areas of the photocatalysts were determined using nitrogen absorption data obtained at liquid nitrogen temperature using the Barrett−Emmett−Teller (BET) technique (Gemini V, Micromeritics).

Photocatalytic activity was evaluated by measuring the oxidation of acetaldehyde to carbon dioxide under visible-light irradiation. Acetaldehyde is a typical VOC pollutant and was used as the probe molecule for evaluating the performance of photocatalysts in the present study. For the measurement, 0.1 g of powder form photocatalyst was uniformly dispersed on a circular glass dish, which was then mounted in a 0.5 L cylindrical glass static reactor equipped with a quartz window. After filling the reaction vessel with an O_2 (20%)−N_2 mixture adjusted to a relative humidity of 10%, acetaldehyde vapor was introduced into the reactor by syringe until the concentration reached approximately 100 ppm. The sample was illuminated under a 150 W Xe lamp (LA-410UV, Hayashi Watch Works Ltd.) equipped with a UV-cutoff filter (Y-43, Asahi

Technoglass) at a light intensity of 30 mW/cm^2. The concentrations of acetaldehyde and CO_2 were measured using a micro gas chromatograph equipped with a thermal conductive detector (TCD, type 3000 with OV-1 and PLOT-U modules, Inficon Ltd.).

RESULTS AND DISCUSSION

The crystal structures of the synthesized photocatalytic samples were investigated by XRD analysis (Figure 1). The XRD pattern of CFO powder matched well with the documented XRD data of $CaFe_2O_4$ (JCPDS card no. 32-0168), indicating

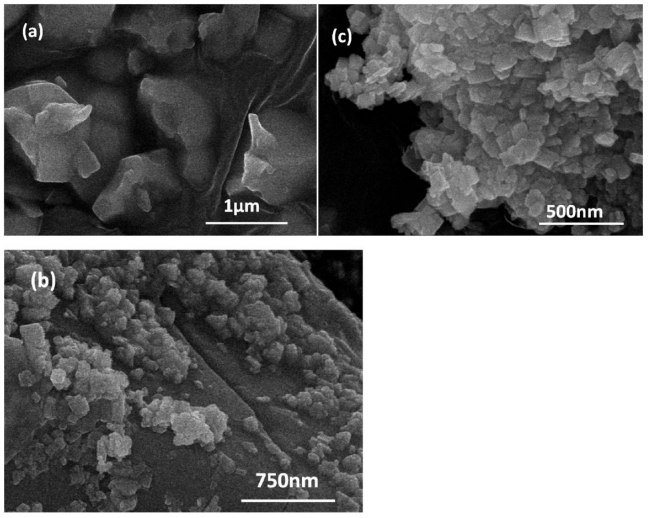

Figure 2. SEM images of CFO (a), CFO/WO_3(H) (b), and CFO/WO_3(M) (c). The weight percentage of CFO in CFO/WO_3(H) and CFO/WO_3(M) was 10%.

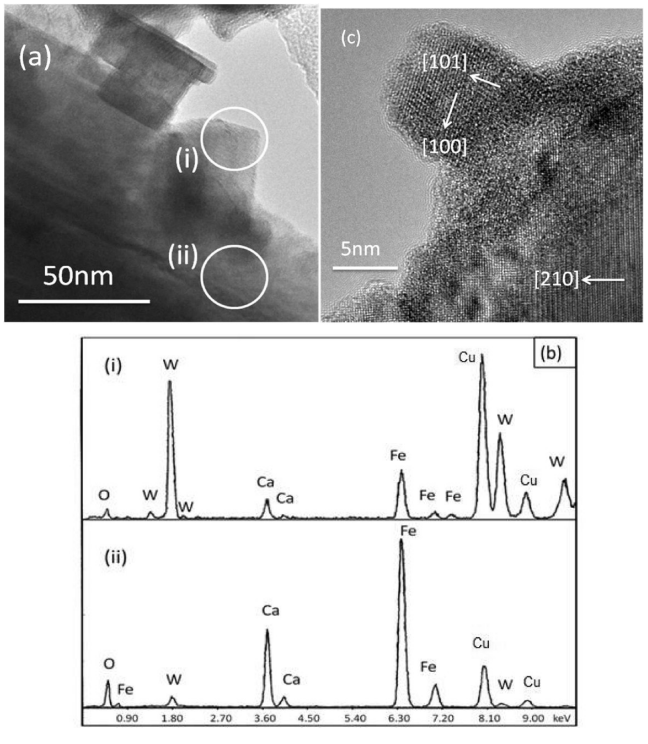

Figure 3. TEM images for CFO/WO_3(H) (a), EDX point analysis for points i and ii in panel a (b), and high-resolution TEM image of CFO/WO_3(H) (c). The weight percentage of CFO in CFO/WO_3(H) was 10%.

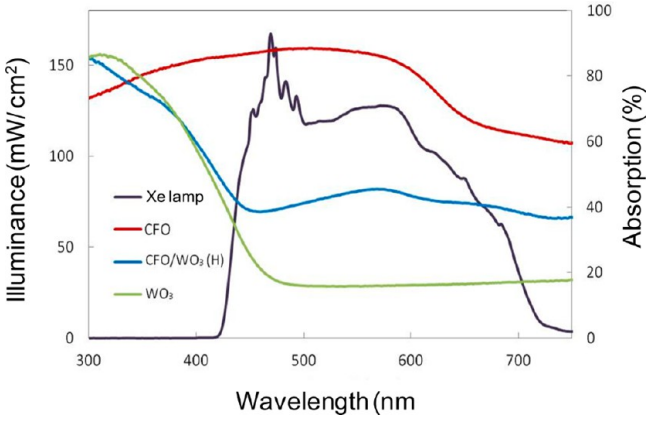

Figure 4. UV−vis spectra for the CFO, WO_3, and CFO/WO_3 powders measured in diffuse reflectance mode and the spectrum of an Xe lamp measured with a UV-cutoff filter (Y-43). The weight percentage of CFO in CFO/WO_3(H) was 10%, which was the optimum amount for the photocatalytic activity.

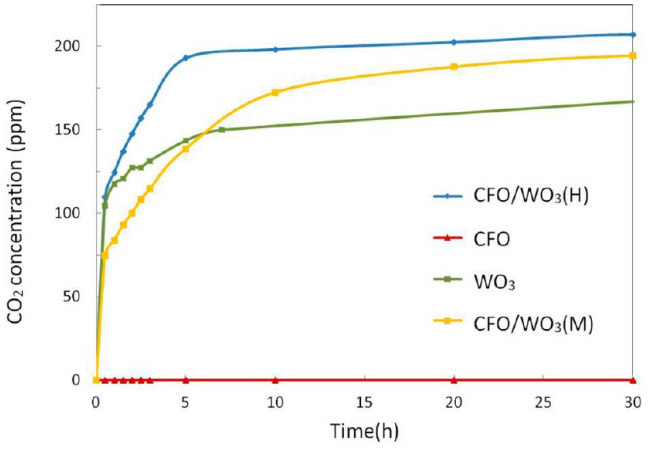

Figure 5. Changes in CO_2 concentration due to the decomposition of acetaldehyde by the CFO, WO_3, and CFO/WO_3 powders as a function of irradiation time under visible light (Xe lamp with a UV-cutoff filter). The weight percentage of CFO in CFO/WO_3(H) was 10%.

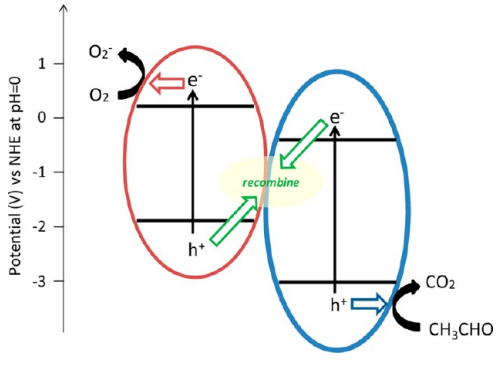

Figure 6. Z-scheme diagram of the CFO/WO_3 composite.

Table 1. Estimated Quantum Yields (QYs) for the Two Types of CFO/WO_3 Composites

composite	QY step 1 (%)	QY step 2 (%)
CFO/WO_3(H)	1.484	0.1277
CFO/WO_3(M)	1.019	0.0863

dx.doi.org/10.1021/am402929d | ACS Appl. Mater. Interfaces 2013, 5, 9770−9776

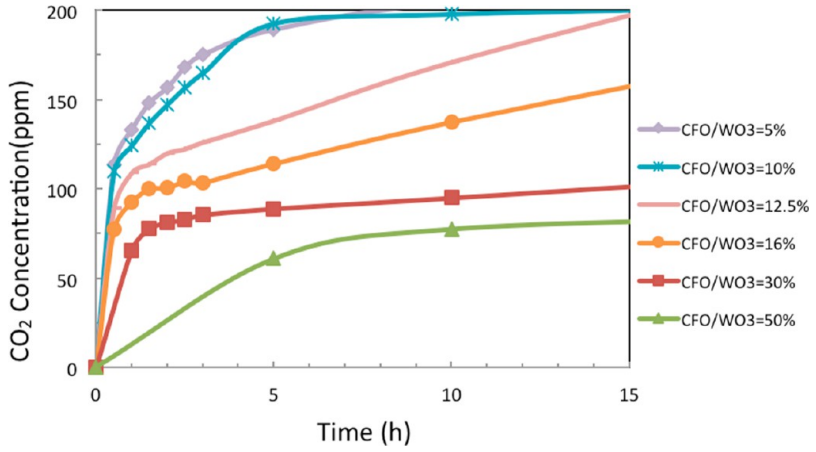

Figure 7. Changes in CO_2 concentration due to the decomposition of acetaldehyde by the CFO/WO_3(H) composite with various ratios of CFO as a function of irradiation time under visible light (Xe lamp with UV cutoff filter). Weight percentages of CFO in CFO/WO_3(H) were 5%, 10%, 12.5%, 16%, 30%, 50%.

that well-crystallized single-phase CFO was obtained. In addition, all XRD peaks for WO_3 could be readily indexed as the crystalline monoclinic form of WO_3 (JCPDS no. 43-1035). The XRD pattern of CFO/WO_3(H) contained all of the peaks observed in the CFO and WO_3 patterns. The half widths of peaks in the CFO/WO_3(H) XRD pattern were similar to those of pure CFO and WO_3, and no peak shifts were observed by the combination of the two semiconductors, excluding the possibility that a solid solution formed between CFO and WO_3. The weight percentage of CFO in the CFO/WO_3 composite used for XRD analysis was 10%, which was optimized for the photocatalytic decomposition of acetaldehyde, as discussed later. The crystallite sizes of CFO and WO_3 were determined using Scherrer's equation ($D_p = 0.9\lambda/(\beta_{1/2} \cos \theta)$, where D_p is the average crystallite size in Å, $\beta_{1/2}$ is the full width of the peak at half-maximum, and θ is the diffraction angle. The calculated crystalline sizes of CFO and WO_3 were 27 and 33 nm, respectively. Analysis of the XRD pattern of CFO/WO_3(M) showed that the crystallinity of the mechanically mixed composite was identical to that of CFO/WO_3(H). These results revealed that the crystallinities of WO_3 and CFO were almost identical in all samples. In addition, the BET surface area for CFO/WO_3(H) and CFO/WO_3(M) was 12.9 and 14.8 m^2/g, respectively, indicating that the surface area did not markedly differ between these samples.

Figure 2 shows SEM images for CFO, CFO/WO_3(H), and CFO/WO_3(M). CFO particles had a grain size in the micrometer range and had a smooth surface. The observed size of CFO grains is markedly larger than the size determined by XRD analysis, which indicated that the CFO particles are polycrystalline with a small crystallite size of approximately 30 nm. Small crystallites were also observed in the CFO/WO_3 composites and were determined to be WO_3 particles based on the TEM results described below. Notably, the WO_3 particles were abundantly attached and highly distributed on the surface of CFO particles in CFO/WO_3(H), whereas numerous WO_3 particles formed aggregates in CFO/WO_3(M).

The CFO/WO_3(H) composite was also analyzed by TEM, which revealed that small block-shaped particles with sizes less than 50 nm were deposited on larger particles (Figure 3). Energy dispersive X-ray spectroscopy (EDX) point analysis was carried out at two points (i and ii) in the TEM image using a 25 nm electron beam (Figure 3b). Copper (Cu) signals in the EDX spectrum for both points i and ii originated from the mesh grid used for the analysis. Strong signals for tungsten (W) were seen in the spectrum for point i, whereas those for calcium (Ca) and iron (Fe) were observed in the spectrum for point ii, indicating that the block-shaped crystallites with a size of 30 nm were WO_3, a finding that is consistent with the size determined in the XRD analysis using Scherrer's equation. Crystal lattice fringes were observed by high-resolution TEM (Figure 3c), and the distances matched well with the (101) and (100) planes of WO_3 and the (210) plane of CFO. These results indicate that highly crystallized WO_3 particles were attached on the surface of CFO crystals.

To promote the selective nucleation of WO_3 particles on the surface of CFO, we attempted to optimize the hydrothermal conditions. The pH of the aqueous solution used for the synthesis of WO_3 particles was near-neutral to cause heterogeneous nucleation on the surface of CFO particles. When WO_3 particles were synthesized at an acidic pH, however, WO_3 particles were homogeneously nucleated and remained in solution as free particles. Under acidic conditions, WO_3 particles were not effectively attached on the CFO surface, and the photocatalytic activity of the resulting composite was much lower than the optimized samples synthesized under neutral pH conditions.

Figure 4 shows UV−vis spectra for the CFO, WO_3, and CFO/WO_3 powders. CFO and WO_3 exhibited band-to-band excitations involving direct and indirect transitions, respectively. Therefore, the band gap of CFO can be estimated according to the energy dependence relation of $\alpha^2(h\nu) \propto (h\nu - E_g)$, while that of WO_3 can be estimated by the relation of $\alpha^{1/2}(h\nu) \propto (h\nu - E_g)$, where α is the absorption coefficient and E_g is the energy gap of a semiconductor (Figure S2). The reported band gap of CFO is 1.9 eV,[27] while that of WO_3 is 2.5−2.8 eV.[32−34] The band gaps determined from the present absorption spectra analysis for CFO and WO_3 are consistent with the previously reported values. It was also observed that the broad absorption of CFO in the visible-light region matched well the spectrum of a Xe lamp. The spectrum of the CFO/WO_3(H) composite appeared to be the added spectra of the single-component powders of CFO and WO_3. We also calculated the absorbed photon numbers in the CFO/WO_3(H) composite (the weight percentage of CFO in CFO/WO_3(H) was 10%) under Xe-lamp irradiation with an initial photon flux of 8.40×10^{16}

(quanta $s^{-1}\cdot cm^2$). Under this light illumination condition, the number of absorbed photons in the CFO component was 6.79×10^{16} (quanta $s^{-1}\cdot cm^2$), whereas that of WO_3 was 1.45×10^{16} (quanta $s^{-1}\cdot cm^2$). We have also investigated the UV−vis spectrum of CFO/WO_3, which prepared using a mechanical method. Its spectrum was consistent with that of CFO/WO_3, which prepared using controlled hydrothermal conditions.

The photocatalytic activity of the CFO/WO_3 composites was evaluated by measuring the decomposition of gaseous acetaldehyde under visible-light irradiation. Figure 5 shows the amount of CO_2 generated resulting from acetaldehyde oxidation as a function of visible-light irradiation time. The initial concentration of acetaldehyde was 100 ppm; thus, the CO_2 concentration was expected to reach 200 ppm if the acetaldehyde was completely decomposed because one acetaldehyde molecule contains two carbon atoms. No CO_2 was generated by pure CFO because the valence band of CFO is not sufficiently positive to oxidize acetaldehyde. In the case of pure WO_3, CO_2 generation was observed, but the CO_2 concentration became saturated around 150 ppm, indicating that pure WO_3 did not completely decompose acetaldehyde into CO_2. In contrast, both CFO/WO_3 composites completely decomposed acetaldehyde to CO_2 under visible-light irradiation. Further, we have investigated the photocatalytic activity of the $WO_3/CaFe_2O_4$ composite under the light with long wavelength ($\lambda > 600$ nm) by using an optical cutoff filter (R-60, Asahi Techno Grass Ltd.). Then the activity under this condition was negligible. These experimental results indicate that the excitations of both semiconductors are indispensable to decompose acetaldehyde completely to carbon dioxide.

The photocatalytic decomposition of acetaldehyde by TiO_2 is reported to proceed by a radical-chain mechanism.[39,40] Although photogenerated holes can directly oxidize acetaldehyde molecules, the activation of oxygen by photogenerated electrons is also critical for the complete oxidation of acetaldehyde to CO_2 and H_2O.[40] As the conduction band of pure WO_3 is more positive than that of TiO_2, WO_3 cannot induce the one-electron reduction of surface-adsorbed oxygen molecules. Further, WO_3 is well-known to cause photochromic reactions. Specifically, photogenerated electrons in the conduction band of WO_3 reduce WO_3 itself, resulting in the formation of color centers such as W^{5+} or W^{4+} species.[41,42] This photochromic reaction is also one of the reasons for the limited photocatalytic activity of pure WO_3. In the CFO/WO_3 composites, however, Z-scheme photocatalytic reactions proceeded under visible-light irradiation; i.e., photogenerated electrons in the conduction band of WO_3 recombined with holes in the valence band of CFO.

Figure 6 shows the band diagram of the CFO/WO_3 system. It has been reported that the conduction band of CFO is sufficiently negative to generate H_2 through the water-splitting reaction,[24] whereas that of WO_3 is more positive than the redox potential required for H_2 generation.[26] However, the oxidation power of holes in the valence band of WO_3 is strong enough to produce O_2 from water,[11] as well as oxidize organic contaminants.[25] In contrast, holes in the valence band of CFO have a lower energy and cannot oxidize organic contaminants, as shown by the inability to decompose acetaldehyde in Figure 5. In our CFO/WO_3 system, electrons with a high reduction potential in the conduction band of CFO react with oxygen molecules in air, while holes with high oxidation power in the valence band of WO_3 react with acetaldehyde molecules. We previously conducted X-ray photoelectron spectroscopy (XPS) for pure WO_3 and CFO/WO_3 composite after light irradiation and observed the reduced species of tungsten ions in the pure WO_3, while the tungsten ions in the CFO/WO_3 composite were very stable.[25] These results also support the conclusion that Z-scheme reactions proceed in the CFO/WO_3 composite. Most notably, the CO_2 generation rate of CFO/WO_3(H) was markedly faster than that of CFO/WO_3(M) (Figure 5). The present experiments were performed using light-limited conditions,[43] under which the electron−hole separation efficiency of the photocatalyst strongly influences its activity.

The profile of CO_2 generation by the CFO/WO_3 composite, as shown in Figure 5, can be divided into two steps. First, acetaldehyde molecules are directly oxidized, followed by the second radical chain reaction and/or oxidation of intermediates, such as acetic acid.[40] We estimated the quantum efficiencies of both reaction steps for the CFO/WO_3(H) and CFO/WO_3(M) composites (see Supporting Information, Figure S3). Table 1 shows that the estimated quantum efficiencies of CFO/WO_3(H) were higher for both steps compared to the CFO/WO_3(M). Previous studies reported that CFO exhibits p-type conductivity, whereas WO_3 has n-type properties.[22,24,27] The improved photocatalytic activity of CFO/WO_3(H) compared to CFO and WO_3 alone is explained by the good junctions formed between the two semiconductors.

We also investigated the influence of hydrothermal conditions on the photocatalytic reaction rate of the CFO/WO_3 composite. Measurement of the surface ζ potential of CFO revealed that the pH value for the isoelectric point of CFO was approximately 1.5 (Figure S4, Supporting Information). We used a neutral pH for the hydrothermal synthesis of WO_3. Under this condition, the CFO surface is negatively charged and efficiently adsorbs cation species in aqueous solution. Further, a mild neutral condition is effective for avoiding the homogeneous formation of WO_3 particles away from the surface of CFO particles. Thus, mild neutral conditions were expected to promote the selective nucleation of WO_3 particles on the surface of CFO. Consistent with this speculation, the photocatalytic activity of the CFO/WO_3 composite synthesized at neutral pH was higher than that synthesized under acidic conditions (see the Supporting Information, Figure S5). Under alkaline conditions, tungsten ions are soluble, making it more difficult to nucleate WO_3 particles. Therefore, near-neutral conditions were used to deposit WO_3 on the surface of CFO.

We also investigated the optimum ratio of CFO and WO_3 in the CFO/WO_3 composite for the visible-light photocatalytic reaction. Figure 7 shows the photocatalytic visible-light activities for the CFO/WO_3(H) composite with various ratios of CFO and WO_3. Composites with 5 or 10 wt % of CFO exhibited the highest photocatalytic activities. When the weight percentage of CFO in CFO/WO_3(H) was 10%, the number of absorbed photons in the CFO component was 6.79×10^{16} ($s^{-1}\cdot cm^2$), whereas that in WO_3 was 1.45×10^{16} ($s^{-1}\cdot cm^2$). The number of absorbed photons in CFO was 3.6 times larger than that in WO_3, even though the ratio of CFO in CFO/WO_3(H) was smaller than that of WO_3, a property that is reflected in the broad visible-light absorption capacity of CFO. The adsorption of a higher number of photons by CFO under the optimized conditions was likely due to differences in the mobility of charge carriers and particle sizes between CFO and WO_3. As CFO has a larger particle size than that of WO_3, charge carriers in CFO must migrate for longer distances to recombine with

carriers at the interface, and therefore, CFO would have more absorbed photons than WO_3. When the CFO content versus WO_3 is larger than 10%, the optimum absorbed photon numbers in two semiconductors become off-balanced for an efficient Z-scheme reaction.

CONCLUSION

In the present study, the n-type semiconductor WO_3 and p-type semiconductor $CaFe_2O_4$ were used as a model system to demonstrate that the selective deposition of heterogeneous semiconductor particles is effective for developing Z-scheme type photocatalysts. By use of controlled hydrothermal conditions, WO_3 nanoparticles were selectively deposited on the surface of CFO, and the synthesized CFO/WO_3 composite exhibited a relatively rapid photocatalytic reaction rate for the decomposition of gaseous acetaldehyde under visible-light irradiation, owing to efficient charge recombination through the junctions that formed between the two semiconductors. Our concept of constructing good junctions between two semiconductors using a controlled hydrothermal reaction is not limited to CFO and WO_3, but rather, it represents a general strategy for developing new visible-light-sensitive Z-scheme photocatalysts.

ASSOCIATED CONTENT

Supporting Information

Figure S1 showing SEM image by probing reflected electrons, Figure S2 showing band gap estimation, Figure S3 showing determination of quantum efficiencies, Figure S4 showing ζ potential for CFO/WO_3 composites, and Figure S5 showing photocatalytic activity of the sample synthesized under acidic conditions. This material is available free of charge via the Internet at http://pubs.acs.org.

AUTHOR INFORMATION

Corresponding Author

*E-mail: mmiyauchi@ceram.titech.ac.jp.

Notes

The authors declare no competing financial interest.

ACKNOWLEDGMENTS

This work was supported by the Advanced Catalytic Transformation Program for Carbon Utilization, Japan Science and Technology Agency (ACT-C, JST). We also thank A. Genseki of the Center for Advanced Materials Analysis at the Tokyo Institute of Technology for assistance with the TEM observations. We also express gratitude to G. Newton for a careful reading of the manuscript.

ABBREVIATIONS

CFO, pure $CaFe_2O_4$
WO_3, pure WO_3
CFO/WO_3(H), hydrothermally synthesized $CaFe_2O_4$/WO_3
CFO/WO_3(M), mechanically mixed $CaFe_2O_4$/WO_3

REFERENCES

(1) Honda, K.; Fujishima, A. *Nature* **1972**, *238*, 37−38.
(2) Hoffmann, H. R.; Martin, S. T.; Choi, W.; Bahnemann, D. W. *Chem. Rev.* **1995**, *95*, 69−96.
(3) Linsebigler, A.; Lu, L. G.; Yates, J. T. *Chem. Rev.* **1995**, *95*, 735−758.
(4) Maeda, K.; Domen, K. *J. Phys. Chem. Lett.* **2010**, *1*, 2655−2661.
(5) Kudo, A.; Miseki, Y. *Chem. Soc. Rev.* **2009**, *38*, 253−278.
(6) Sato, S.; Morikawa, T.; Saeki, S.; Kajino, T.; Motohiro, T. *Angew. Chem., Int. Ed.* **2010**, *49*, 5101−5105.
(7) Wang, R.; Hashimoto, K.; Fujishima, A.; Chikuni, M.; Kojima, E.; Kitamura, A.; Shimohigoshi, M.; Watanabe, T. *Nature* **1997**, *388*, 431−432.
(8) Qiu, X.; Miyauchi, M.; Sunada, K.; Minoshima, M.; Liu, M.; Lu, Y.; Li, D.; Shimodaira, Y.; Hosogi, Y.; Kuroda, Y.; Hashimoto, K. *ACS Nano* **2012**, *6*, 1609−1618.
(9) Torimoto, T.; Nakamura, N.; Ikeda, S.; Ohtani, B. *Phys. Chem. Chem. Phys.* **2002**, *4*, 5910−5914.
(10) Kaur, P.; Sud, D. *J. Mol. Catal. A: Chem* **2012**, *365*, 32−38.
(11) Sayama, K.; Mukasa, K.; Abe, R.; Abe, Y.; Arakawa, H. *Chem.Commun.* **2001**, *23*, 2416−2417.
(12) Abe, R.; Sayama, K.; Sugihara, H. *J. Phys. Chem. B* **2005**, *109*, 16052−16061.
(13) Sasaki, Y.; Nemoto, H.; Saito, K.; Kudo, A. *J. Phys. Chem. C* **2009**, *113*, 17536−17542.
(14) Higashi, M.; Abe, R.; Ishikawa, A.; Takata, T.; Ohtani, B.; Domen, K. *Chem. Lett.* **2008**, *37*, 138−139.
(15) Hara, S.; Yoshimizu, M.; Tanigawa, S.; Ni, L.; Ohtani, B.; Irie, H. *J. Phys. Chem. C* **2012**, *116*, 17458−17463.
(16) Sato, S.; Arai, T.; Morikawa, T.; Uemura, K.; Suzuki, T. M.; Tanaka, H.; Kajino, T. *J. Am. Chem. Soc.* **2011**, *133*, 15240−15243.
(17) Sekizawa, K.; Maeda, K.; Domena, K.; Koike, K.; Ishitani, O. *J. Am. Chem. Soc.* **2013**, *135*, 4596−4599.
(18) Wang, X.; Li, S.; Ma, Y.; Yu, H.; Yu, J. *J. Phys. Chem. C* **2011**, *115*, 14648−14655.
(19) Kim, H. G.; Borse, P. H.; Choi, W.; Lee, J. S. *Angew. Chem., Int. Ed.* **2005**, *44*, 4585−4589.
(20) Tada, H.; Mitsui, T.; Kiyonaga, T.; Akita, T.; Tanaka, K. *Nat. Mater.* **2006**, *5*, 782−786.
(21) Zhang, L. S.; Wong, K. H.; Chen, Z. G.; Yu, J. C.; Zhao, J. C.; Hu, C.; Chan, C. Y.; Wong, P. K. *Appl. Catal., A* **2009**, *363*, 221−229.
(22) Arai, T.; Yanagida, M.; Konishi, Y.; Iwasaki, Y.; Sugihara, H.; Sayama, K. *J. Phys. Chem. C* **2007**, *111*, 7574−7577.
(23) Arai, T.; Yanagida, M.; Konishi, Y.; Iwasaki, Y.; Sugihara, H.; Sayama, K. *Catal. Commun.* **2008**, *9*, 1254−1258.
(24) Ida, S.; Yamada, K.; Matsunaga, T.; Hagiwara, H.; Matsumoto, Y.; Ishihara, T. *J. Am. Chem. Soc.* **2010**, *132*, 17343−17345.
(25) Liu, Z.; Zhao, Z.; Miyauchi, M. *J. Phys. Chem. C* **2009**, *113*, 17132−17137.
(26) Liu, Z.; Miyauchi, M. *Chem. Commun.* **2009**, *15*, 2002−2004.
(27) Matsumoto, Y. *J. Solid State Chem.* **1996**, *126*, 227−234.
(28) Kim, H. G.; Borse, P. H.; Jang, J. S.; Jeong, E. D.; Jung, O.; Suh, Y. J.; Lee, J. S. *Chem. Commun.* **2009**, 5889−5891.
(29) Borse, P. H.; Kim, J. Y.; Lee, J. S.; Lim, K. T. *J. Korean Phys. Soc.* **2011**, *61*, 73−79.
(30) Cao, J.; Kako, T.; Li, P.; Ouyang, S.; Ye, J. *Electrochem. Commun.* **2011**, *13*, 275−278.
(31) Kim, E. S.; Nishimura, N.; Magesh, G.; Kim, J. Y.; Jang, J. W.; Jun, H.; Kubota, J.; Domen, K.; Lee, J. S. *J. Am. Chem. Soc.* **2013**, *135*, 5375−5383.
(32) Sclafani, A.; Palmisano, L.; Marci, G.; Venezia, A. *Sol. Energy Mater. Sol. Cells* **1998**, *51*, 203−219.
(33) Bamwenda, G. R.; Arakawa, H. *Appl. Catal., A* **2001**, *210*, 181−191.
(34) Darwent, J. R.; Mills, A. *J. Chem. Soc., Faraday Trans.* **1982**, *78*, 359−367.
(35) Abe, R.; Takami, H.; Murakami, N.; Ohtani, B. *J. Am. Chem. Soc.* **2008**, *130*, 7780−7781.
(36) Irie, H.; Miura, S.; Kamiya, K.; Hashimoto, K. *Chem. Phys. Lett.* **2008**, *457*, 202−205.
(37) Zhao, Z.; Miyauchi, M. *Angew. Chem., Int. Ed.* **2008**, *120*, 7159−7163.
(38) Anandan, S.; Miyauchi, M. *Chem. Commun.* **2012**, *48*, 4323−4325.
(39) Pelizzetti, Z.; Minero, C. *Electrochim. Acta* **1993**, *38*, 47−55.
(40) Ohko, Y.; Tryk, D. A.; Hashimoto, K.; Fujishima, A. *J. Phys. Chem. B* **1998**, *102*, 2699−2704.

(41) Bechinger, C.; Oefinger, G.; Herminghaus, S.; Leiderer, P. *J. Appl. Phys.* **1993**, *74*, 4527−4533.
(42) Chang, I. F.; Gilbert, B. L.; Sun, T. I. *J. Electrochem. Soc.* **1975**, *122*, 955−962.
(43) Ohko, Y.; Hashimoto, K.; Fujishima, A. *J. Phys. Chem. A* **1997**, *101*, 8057−8062.